Large-N-approximated field theory for multipartite entanglement

P. Facchi,[1,2] G. Florio,[1,2,3,4] G. Parisi,[5,6,7] S. Pascazio,[1,2] and A. Scardicchio[8,9,1]
[1]*Dipartimento di Fisica and MECENAS, Università di Bari, I-70126 Bari, Italy*
[2]*INFN, Sezione di Bari, I-70126 Bari, Italy*
[3]*Museo Storico della Fisica e Centro Studi e Ricerche "Enrico Fermi", Piazza del Viminale 1, I-00184 Roma, Italy*
[4]*Dipartimento di Meccanica, Matematica e Management, Politecnico di Bari, Via E. Orabona 4, 70125 Bari, Italy*
[5]*Dipartimento di Fisica, Università di Roma "Sapienza", Piazzale Aldo Moro 2, I-00185 Roma, Italy*
[6]*Centre for Statistical Mechanics and Complexity (SMC), CNR-INFM, I-00185 Roma, Italy*
[7]*INFN, Sezione di Roma, I-00185 Roma, Italy*
[8]*International Center for Theoretical Physics, Strada Costiera 11, 34151 Trieste, Italy*
[9]*INFN, Sezione di Trieste, I-34151, Trieste, Italy*
(Received 19 June 2015; published 16 December 2015)

We try to characterize the statistics of multipartite entanglement of the random states of an n-qubit system. Unable to solve the problem exactly we generalize it, replacing complex numbers with real vectors with N_c components (the original problem is recovered for $N_c = 2$). Studying the leading diagrams in the large-N_c approximation, we unearth the presence of a phase transition and, in an explicit example, show that the so-called entanglement frustration disappears in the large-N_c limit.

DOI: 10.1103/PhysRevA.92.062330 PACS number(s): 03.67.Mn, 05.70.Fh, 64.60.Bd, 03.65.Aa

I. INTRODUCTION

The study of entanglement is almost as old as quantum mechanics, as it was the subject of seminal papers by Einstein, Podolsky, and Rosen [1] and Schrödinger [2]. The focus of the founding fathers was on the puzzling, nonclassical aspects of quantum correlations. Nowadays, entanglement [3–5] is viewed mostly as a crucial resource in quantum applications, quantum communication, and quantum information processing [6], and it maintains its original fascination for the comprehension of the structure and geometry of quantum mechanics [7].

While bipartite entanglement is well understood and quantified, the notion of multipartite entanglement is more elusive. This is due to a number of concomitant factors. First of all, for many-body quantum systems, the number of entanglement measures grows exponentially with the system size [8], making a characterization of quantum correlations complicated [9]. Second, new properties arise when more quantum parties are involved, among these the intriguing appearance of frustration. In agreement with the classical notion [10], this is related to the impossibility of satisfying a number of requirements at the same time [11]. Applied to entanglement, this means that given three (or more) parties A, B, and C, if the entanglement between A and B grows, that between A and C or B and C decreases. This is also referred to as "monogamy" of entanglement [12–14].

In our work the symptoms of such frustration will surface in the investigation of $n = 4$ qubits [15–17] and for small number of qudits [18–22], and cannot be avoided for $n \geqslant 8$ qubits, where one can prove that it is impossible to maximize the bipartite entanglement by maximizing independently all possible bipartitions of a system of qubits [23–25]. Further interesting contributions to these problems were given in Refs. [26,27].

In this article we will study the properties of multipartite entanglement by adopting the concepts and tools of classical statistical mechanics [28–31]. This approach has proved useful in the study of the bipartite entanglement of a large number of qubits, where it unearths the presence of phase transitions [32,33]. The situation with multipartite entanglement is, however, much more complex. This is due to the fact that the monogamy of entanglement acts effectively as a frustration, and the resulting statistical system is frustrated, to say, similarly to a spin glass.

In order to explore the rich landscape that ensues, we shall make use of techniques that are based on the analysis of diagrams that naturally arise when one considers a high-temperature expansion of the distribution function of the measure of multipartite entanglement (the potential of multipartite entanglement) [29]. Unfortunately, the evaluation of the contributions of different kinds of graphs and their resummation is not a simple task. Following a procedure familiar from gauge theories, one would like to find a strategy to select and sum a family of diagrams which dominate the result in one particular limit.

By following this route we will be able to give a more general formulation of this problem, replacing the (complex) coefficients of the wave function with N_c-dimensional real vectors. When N_c is viewed as a "color" index, the original formulation in terms of qubits will be recovered when $N_c = 2$. This generalization appears in a natural way by analyzing the mathematical structure of the measure used to characterize the multipartite entanglement. Clearly, the physics of the case $N_c \gg 2$ will not be the same as in the original problem $N_c = 2$, however, as it is often the case with large-N_c expansions, the two problems share some important ingredients and salient features. Fundamentally, we hope to understand whether the phase transitions that are known to appear in the bipartite case [32,33] are present in the statistics of multipartite entanglement.

We will see that these expectations are correct: the symptoms of a phase transition are present even for multipartite entanglement: there is a phase transition in the limit of large N_c. Moreover, we will see an explicit example where the frustration of multipartite entanglement disappears if the value

of N_c is large enough. This simplification for large N_c is common in statistical models and field theories.

This article is organized as follows. In Sec. II we introduce notation and familiarize with the statistical mechanics approach we will use. In Sec. III we build the diagrammatics and evaluate the first relevant cumulants of the theory. We introduce the color index N_c in Sec. IV, and look at the limit of large number of colors: this enables us to restrict our attention to an interesting class of diagrams. As a consequence, we can investigate the behavior of the entanglement for large values of N_c in Sec. V: this unveils the presence of a phase transition that is studied in Sec. VI A. The phase transition is further investigated in Sec. VI B, where we numerically show that no hysteresis appears. We conclude in Sec. VII with a few comments.

II. MULTIPARTITE ENTANGLEMENT AND STATISTICAL MECHANICS

A. Potential of multipartite entanglement

Let us consider an ensemble $S = \{1,2,\dots,n\}$ of n qubits in the Hilbert space $\mathcal{H}_S = (\mathbb{C}^2)^{\otimes n}$. In this article we will focus on pure states

$$|z\rangle = \sum_{k\in\mathbb{Z}_2^n} z_k |k\rangle, \quad z_k \in \mathbb{C}, \quad \sum_{k\in\mathbb{Z}_2^n} |z_k|^2 = 1, \tag{2.1}$$

where $z = (z_k)$, $k = (k_i)_{i\in S}$, $k_i \in \mathbb{Z}_2 = \{0,1\}$, and

$$|k\rangle = \bigotimes_{i\in S} |k_i\rangle_i, \quad |k_i\rangle_i \in \mathbb{C}^2, \quad \langle k_i|k_j\rangle = \delta_{ij}. \tag{2.2}$$

Consider a bipartition $(A,\bar{A})$ of the system, where $A \subset S$ is a subset of n_A qubits and $\bar{A} = S\backslash A$ its complement, with $n_A + n_{\bar{A}} = n$. We set $n_A \leqslant n_{\bar{A}}$ without loss of generality. The total Hilbert space factorizes into $\mathcal{H}_S = \mathcal{H}_A \otimes \mathcal{H}_{\bar{A}}$, with $\mathcal{H}_A = \bigotimes_{i\in A} \mathbb{C}_i^2$, of dimensions $N_A = 2^{n_A}$ and $N_{\bar{A}} = 2^{n_{\bar{A}}}$, respectively ($N_A N_{\bar{A}} = N$).

The *bipartite* entanglement between the two subsets can be measured by the purity of the reduced state of subsystem A,

$$\pi_A(z) = \mathrm{Tr}\rho_A^2, \quad \rho_A = \mathrm{Tr}_{\bar{A}}|\psi\rangle\langle\psi|, \tag{2.3}$$

$\mathrm{Tr}_{\bar{A}}$ being the partial trace over $\bar{A}$. We notice that $\pi_A = \pi_{\bar{A}}$ and

$$1/N_A \leqslant \pi_A \leqslant 1, \tag{2.4}$$

where the lower and upper bounds are obtained for maximally entangled and separable states, respectively.

A natural extension of this measure to the multipartite scenario is realized considering the *potential of multipartite entanglement*, that is the average bipartite entanglement between balanced bipartitions [24]:

$$\begin{aligned} H(z) &= \binom{n}{n_A}^{-1} \sum_{|A|=n_A} \pi_A(z) \\ &= \sum_{k,k',l,l'\in\mathbb{Z}_2^n} \Delta(k,k';l,l')\, z_k\, z_{k'}\, \bar{z}_l\, \bar{z}_{l'}\,, \end{aligned} \tag{2.5}$$

where $n_A = [n/2]$ (balanced bipartitions), with $[x]$ being the integer part of x. The *coupling function* is [25,30]

$$\Delta(k,k';l,l') = g((k\oplus l)\vee(k'\oplus l'),(k\oplus l')\vee(k'\oplus l)), \tag{2.6}$$

where

$$g(a,b) = \delta_{a\wedge b,0}\ \hat{g}(|a|,|b|) \tag{2.7}$$

and

$$\hat{g}(s,t) = \frac{1}{2}\binom{n}{n_A}^{-1}\left[\binom{n-s-t}{n_A-s} + \binom{n-s-t}{n_A-t}\right]. \tag{2.8}$$

In Eqs. (2.6) and (2.7) we have defined $|a| = \sum_{i\in S} a_i$, $|b| = \sum_{i\in S} b_i$, $a\oplus b = (a_i + b_i \bmod 2)_{i\in S}$ being the XOR operation, $a\vee b = (a_i + b_i - a_i b_i)_{i\in S}$ the OR operation, and $a\wedge b = (a_i b_i)_{i\in S}$ the AND operation. Due to its linear structure, $H(z)$ inherits the upper and lower bound of the purity $\pi_A(z)$ in (2.4):

$$1/N_A \leqslant H(z) \leqslant 1. \tag{2.9}$$

We notice the following symmetries of the coupling function:

$$\begin{aligned} \Delta(k,k';l,l') &= \Delta(k',k;l,l'), \\ \Delta(k,k';l,l') &= \Delta(l,l';k,k'), \\ \Delta(k,k';l,l') &= \Delta(k',k;l',l), \end{aligned} \tag{2.10}$$

which reflect the reality of $H(z)$,

$$\overline{H(z)} = H(\bar{z}) = H(z). \tag{2.11}$$

Moreover, since

$$\Delta(k\oplus m,k'\oplus m;l\oplus m,l'\oplus m) = \Delta(k,k';l,l'), \tag{2.12}$$

the potential is invariant under rotations and reflections:

$$H(z_{k\oplus m}) = H(z_k) \tag{2.13}$$

for every $m \in \mathbb{Z}_2^n$.

B. Classical statistical mechanics approach

The analysis of the properties of $H(z)$ can be rephrased in a classical statistical mechanical framework. Let us consider the partition function of a system with Hamiltonian $H(z)$ at a fictitious temperature β^{-1},

$$Z(\beta) = \int e^{-\beta H(z)}\, d\mu(z), \tag{2.14}$$

where [34]

$$d\mu(z) = \frac{(N-1)!}{\pi^N}\,\delta(1-\|z\|^2)\prod_k dz_k d\bar{z}_k \tag{2.15}$$

is the uniform measure on the hypersphere

$$\|z\|^2 = \sum_k |z_k|^2 = 1, \tag{2.16}$$

and $dz_k d\bar{z}_k$ denotes the Lebesgue measure on $\mathbb{C}$.

The Lagrange multiplier β fixes the average value of multipartite entanglement. In particular, $\beta = 0$ corresponds to the uniform sampling of random states. The limits $\beta \to \pm\infty$

select configurations that, respectively, minimize or maximize $H(z)$; the former case corresponds to maximally multipartite entangled states (MMES) [24], the latter to completely separable states.

The average value of $H(z)$ (seen as the average energy of the system) at arbitrary β can be obtained as

$$\langle H\rangle_\beta = \frac{1}{Z(\beta)}\int H\, e^{-\beta H}\, d\mu = -\frac{\partial}{\partial\beta}\ln Z(\beta). \quad (2.17)$$

The properties of the distribution function of the potential of multipartite entanglement can be analyzed by evaluating its cumulants. In particular, the mth cumulant of $H(z)$ reads

$$\kappa_\beta^{(m)} = (-1)^m\frac{\partial^m}{\partial\beta^m}\ln Z(\beta) = (-1)^{m-1}\frac{\partial^{m-1}}{\partial\beta^{m-1}}\langle H\rangle_\beta. \quad (2.18)$$

III. DIAGRAMMATIC EVALUATION OF THE CUMULANTS

In this section we will briefly review some properties of the high temperature expansion of the distribution function of the potential of multipartite entanglement. We remind that for $\beta = 0$ one gets the unbiased random states. The average potential reads

$$\langle H\rangle_\beta = \sum_{m=1}^{\infty}\frac{(-\beta)^{m-1}}{(m-1)!}\kappa_0^{(m)}, \quad (3.1)$$

where the brackets $\langle\cdots\rangle_0$ denote the average with respect to the uniform (unitarily invariant) measure (2.15). The only nonvanishing correlation functions are of the form [30]

$$\left\langle\prod_{j=1}^{N}|z_j|^{2m_j}\right\rangle_0 = \frac{(N-1)!\prod_{j=1}^{N}m_j!}{\left(N-1+\sum_{j=1}^{N}m_j\right)!}, \quad (3.2)$$

where m_j are nonnegative integers. In order to calculate the required cumulants, we will make use of the diagrammatic technique developed in [30]. In this way we will be able to evaluate the contribution arising from different kinds of graphs. The objective of this study is to try to understand whether by embedding this problem in a larger family, dependent on a parameter to be introduced in the following, called N_c, the number of colors, a class of graphs can be isolated that dominate in an appropriate limit. To this extent, we will promote the complex numbers defining the wave functions to real vectors of N_c components and take N_c large. In the following two sections we recall the computations in [30], and we anticipate which diagrams are going to be relevant in the large-N_c limit.

A. First cumulant

The average potential at $\beta = 0$ reads

$$\begin{aligned}\langle H\rangle_0 &= \sum_{k,l\in\mathbb{Z}_2^{2n}}\Delta(k_1,k_2;l_1,l_2)\left\langle z_{k_1}z_{k_2}\bar z_{l_1}\bar z_{l_2}\right\rangle_0\\ &= \langle|z_1|^2|z_2|^2\rangle_0\sum_{p\in\mathcal{S}_2}[p(1)\ p(2)],\end{aligned} \quad (3.3)$$

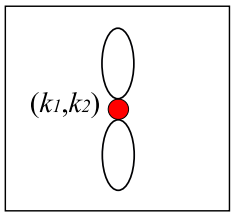

FIG. 1. (Color online) Graph contributing to the first cumulant: two-leaf cactus diagram.

where

$$[p(1)\ p(2)] = \sum_{k_1,k_2\in\mathbb{Z}_2^n}\Delta(k_1,k_2;k_{p(1)},k_{p(2)}) \quad (3.4)$$

and $\mathcal{S}_2$ is the symmetric group of order 2. This is represented by the doubly degenerate graph in Fig. 1 which, by (2.6) and (3.2), gives

$$\langle H\rangle_0 = \frac{N_A+N_{\bar A}}{N+1}. \quad (3.5)$$

For balanced bipartitions of an even number of qubits, $N_A = N_{\bar A} = \sqrt{N}$, and $N\to+\infty$ we get

$$\langle H\rangle_0 = \frac{2\sqrt{N}}{N+1}\sim\frac{2}{\sqrt{N}}. \quad (3.6)$$

For an odd number of qubits the value of $\langle H\rangle_0$ is $3/\sqrt{2}$ larger than (3.6).

B. Second cumulant

The second cumulant is defined as

$$\kappa_0^{(2)} = \langle H^2\rangle_0 - \langle H\rangle_0^2. \quad (3.7)$$

We have

$$\begin{aligned}\langle H^2\rangle_0 &= \sum_{k,l\in\mathbb{Z}_2^{4n}}\Delta(k_1,k_2;l_1,l_2)\Delta(k_3,k_4;l_3,l_4)\\ &\quad\times\left\langle z_{k_1}z_{k_2}z_{k_3}z_{k_4}\bar z_{l_1}\bar z_{l_2}\bar z_{l_3}\bar z_{l_4}\right\rangle_0\\ &= \langle|z_1|^2|z_2|^2|z_3|^2|z_4|^2\rangle_0\sum_{p\in\mathcal{S}_4}[p(1)\ p(2),p(3)\ p(4)].\end{aligned} \quad (3.8)$$

Let us evaluate the contribution from connected graphs. The graph with two links between left and right pairs in Fig. 2 has degeneracy 16 and reads

$$[1\ 3,2\ 4] = \frac{N\,(N_A+N_{\bar A})^2}{4}. \quad (3.9)$$

The graph shown in Fig. 3 has degeneracy 4. The associated contribution does not have a transparent form; on the other

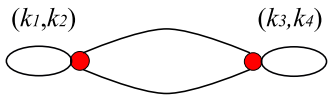

FIG. 2. (Color online) Connected graph contributing to the second cumulant: three-leaf cactus diagram.

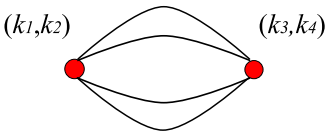

FIG. 3. (Color online) Connected graph without leaves contributing to the second cumulant.

hand, its asymptotic formula reads [30]

$$[3\ 4,1\ 2]\ \sim \frac{3\sqrt{2}}{4}N^{\alpha}, \tag{3.10}$$

with $\alpha = \log_2 3 \simeq 1.5850$.

Notice the presence of the irrational exponent in the graph (3.10). Moreover, since (3.9) is exactly canceled by the nonconnected contribution from the square of (3.5), the graph (3.10) represents the dominant contribution to the second cumulant $\kappa_0^{(2)}$ that therefore has the asymptotic value of

$$\kappa_0^{(2)} \simeq \frac{3\sqrt{2}}{N^{2.4150\ldots}}. \tag{3.11}$$

However, considering only the contribution from the graph (3.9), which will turn out to be dominant in the large-N_c limit (see later in the paper), we obtain

$$\tilde{\kappa}_0^{(2)} = \frac{4(N_A + N_{\bar{A}})^2}{(N+1)(N+2)(N+3)} \sim \frac{16}{N^2}, \tag{3.12}$$

where the asymptotic expression is valid for balanced bipartitions of an even number of qubits, $N_A = N_{\bar{A}} = \sqrt{N}$, and $N \to +\infty$.

C. Third cumulant

The third cumulant reads

$$\begin{aligned}\kappa_0^{(3)} &= \langle (H - \langle H\rangle_0)^3\rangle_0 \\ &= \langle H^3\rangle_0 - 3\langle H^2\rangle_0\langle H\rangle_0 + 2\langle H\rangle_0^3,\end{aligned} \tag{3.13}$$

and we have

$$\begin{aligned}\langle H^3\rangle_0 = {} & \langle |z_1|^2|z_2|^2|z_3|^2|z_4|^2|z_5|^2|z_6|^2\rangle_0 \\ & \times \sum_{p\in\mathcal{S}_6}[p(1)\ p(2),p(3)\ p(4),p(5)\ p(6)].\end{aligned} \tag{3.14}$$

The contributions from connected graphs with three leaves (degeneracy 128), represented in Fig. 4(a), and with two leaves (degeneracy 192), represented in Fig. 4(b), are equal

$$[1\ 6,3\ 2,5\ 4] = [1\ 3,2\ 5,4\ 6] = N\frac{(N_A + N_{\bar{A}})^3}{8} \sim N^{5/2}. \tag{3.15}$$

The graph represented in Fig. 4(c) (degeneracy 192) gives an asymptotic contribution

$$[1\ 6,2\ 5,3\ 4] \sim 3\sqrt{2}N^{\alpha+1/2}. \tag{3.16}$$

Finally, the asymptotic contributions from the graphs in Figs. 5(a) and 5(b) read, respectively [30],

$$[5\ 6,1\ 2,3\ 4] \sim N^{\alpha}, \tag{3.17}$$

$$[3\ 6,5\ 2,1\ 4] \sim cN^{\gamma}, \tag{3.18}$$

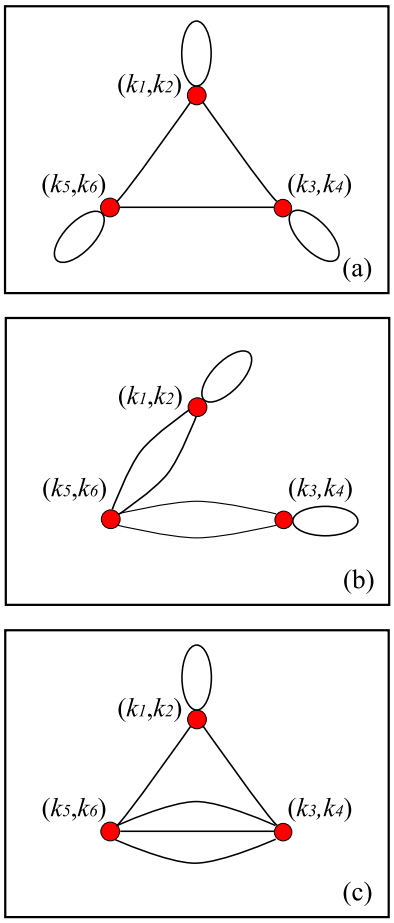

FIG. 4. (Color online) Connected graphs (with leaves) contributing to the second cumulant. (a) Four-leaf cactus diagram. (b) Four-leaf cactus diagram. (c) One leaf.

with $c \simeq 1.05385$ and $\gamma \simeq 1.8417$. Notice the appearance of a new irrational exponent γ, which again, by cancellations, turns out to be the dominant contribution to the cumulant $\kappa_0^{(3)}$, followed by that due to α. In summary, the asymptotic value is

$$\kappa_0^{(3)} \simeq 67.4\ N^{-4.158\ldots}. \tag{3.19}$$

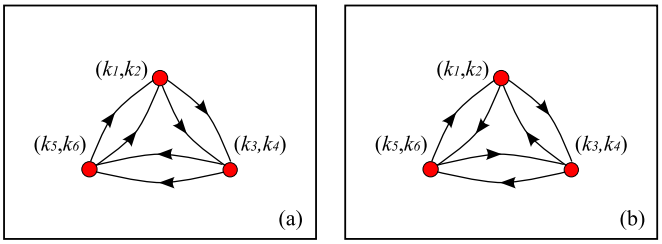

FIG. 5. (Color online) Connected graphs (without leaves) contributing to the second cumulant. (a) Same internal and external orientation of the edges. (b) Opposite internal and external orientation of the edges.

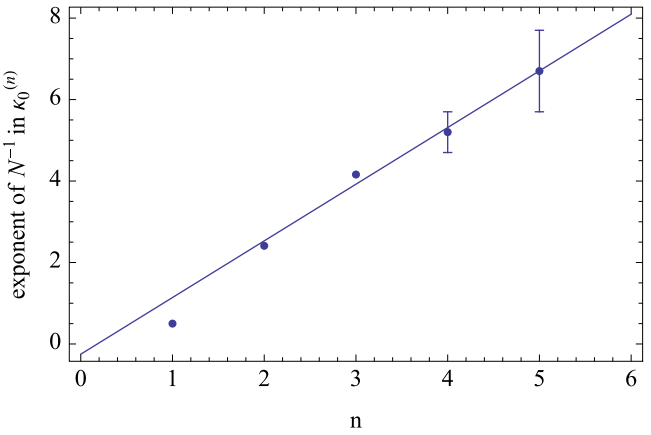

FIG. 6. (Color online) The scaling exponent of κ_n from numerics. On the first three points the error bars are smaller than the symbol size and the data agree with the theory.

Again, by retaining only the contributions from Eq. (3.15), as for $\tilde{\kappa}_0^{(2)}$, which dominate the large-N_c limit we find

$$\tilde{\kappa}_0^{(3)} = \frac{40(N_A+N_{\bar{A}})^3}{(N+1)(N+2)(N+3)(N+4)(N+5)} \sim \frac{320}{N^{7/2}}, \tag{3.20}$$

where the asymptotic expression is obtained for balanced bipartitions of an even number of qubits, $N_A = N_{\bar{A}} = \sqrt{N}$, and $N \to +\infty$.

For the fourth and fifth cumulant we have to resort to numerical methods. By generating a large number of random vectors for different N, we find that

$$\kappa_0^{(3)} = (43 \pm 12)N^{-4.18\pm0.06}, \tag{3.21}$$

$$\kappa_0^{(4)} = (27 \pm 20)N^{-5.2\pm0.5}, \tag{3.22}$$

$$\kappa_0^{(5)} = (148 \pm 90)N^{-6.5\pm1.5}, \tag{3.23}$$

where $\kappa_0^{(3)}$ is in good agreement with the theoretical value [compare (3.21) with (3.19)].

These numbers suggest a scaling of the form $\kappa_0^{(n)} \sim N^{-0.25-1.4n}$ (whose quality can be seen in Fig. 6), in partial agreement with the large-N_c result $\tilde{\kappa}_0^{(n)} \sim N^{1-1.5n}$.

IV. CACTUS DIAGRAMS AND LARGE NUMBER OF COLORS

As the reader should have deduced from the previous sections, the proliferation of diagrams and the variety of the exponents on N prevent one from writing a closed form for the correlation functions $\langle z_i \bar{z}_j \rangle_\beta$. One can then decide to sum a particular family of diagrams, as we did for the second and third cumulant in the high temperature expansion Eqs. (3.12) and (3.20), hoping that this can give some information about the characterization of multipartite entanglement. However, the choice of the cactus (subdominant) diagrams was quite arbitrary and motivated only by the fact that they yield integer exponents.

Of course, one should choose the family of graphs with an objective criterion, not on the basis of ease of computation. An objective criterion, which is common practice in field theory, is that of generalizing the model to a larger symmetry group, from SO(2) to SO(N_c), and then taking the limit of large number of colors N_c [35–37]. This will select a family of diagrams, and enable us to compute their amplitudes in a closed form to leading order in $1/N_c$. We will see that these diagrams are exactly the cactuses. Moreover, we will see, at the end of the computation, that a phase transition is obtained at a temperature below which a combination of the rotation group SO(N_c) and the symmetric group $\mathcal{S}_n$ is spontaneously broken.

In order to perform this calculation, we will rewrite the expression of the potential of multipartite entanglement in a different form. The Fourier coefficients z_k of a quantum state can be written as

$$z_k = \Phi_k^1 + i\Phi_k^2, \tag{4.1}$$

with Φ_k^μ, $\mu = 1,2$, real numbers. We will consider this object as a two components vector. In terms of these real quantities, we can rewrite the potential of multipartite entanglement in Eq. (2.5) in the following form [using the symmetries in Eq. (2.10)]:

$$\begin{aligned} H &= \sum_{k,k',l,l' \in \mathbb{Z}_2^n} \Delta(k,k';l,l') \\ &\quad \times \left[2 \sum_{\mu,\nu=1}^{2} \Phi_k^\mu \Phi_l^\mu \Phi_{k'}^\nu \Phi_{l'}^\nu - \sum_{\mu,\nu=1}^{2} \Phi_k^\mu \Phi_{k'}^\mu \Phi_l^\nu \Phi_{l'}^\nu \right] \\ &= \frac{N_c}{2} \sum_{k,k',l,l' \in \mathbb{Z}_2^n} \tilde{\Delta}(k,k';l,l') \sum_{\mu,\nu=1}^{N_c} \Phi_k^\mu \Phi_l^\mu \Phi_{k'}^\nu \Phi_{l'}^\nu, \end{aligned} \tag{4.2}$$

for $N_c \equiv 2$, and

$$\tilde{\Delta}(k,k';l,l') = 2\Delta(k,k';l,l') - \Delta(k,l;k',l'). \tag{4.3}$$

This expression can be put in a more compact form by writing

$$H = \frac{N_c}{2} \sum_{k,k',l,l' \in \mathbb{Z}_2^n} \tilde{\Delta}(k,k';l,l')(\vec{\Phi}_k \cdot \vec{\Phi}_l)(\vec{\Phi}_{k'} \cdot \vec{\Phi}_{l'}), \tag{4.4}$$

where, in general, $\vec{\Phi}_k = (\Phi_k^1, \ldots, \Phi_k^{N_c})$, and the dot denotes the scalar product. The index μ, ranging from 1 to N_c, will play in the following the role of a *color* index, and we will be interested in the limit $N_c \to \infty$. The normalization of the complex vector z_k becomes, for generic N_c, the constraint

$$\sum_{k \in \mathbb{Z}_2^n} \sum_{\mu=1}^{N_c} \left(\Phi_k^\mu\right)^2 = \sum_{k \in \mathbb{Z}_2^n} \vec{\Phi}_k \cdot \vec{\Phi}_k = 1. \tag{4.5}$$

We will now show that the generalized potential (4.4) is positive for any color N_c, and will find a lower bound which generalizes the bound on the potential of multipartite entanglement, valid for $N_c = 2$. From (2.5) and the explicit expression of the purity across the bipartition $(A, \bar{A})$,

$$\pi_A(z) = \sum_{k,k',l,l'} \delta_{k_A,l'_A} \delta_{k'_A,l_A} \delta_{k_{\bar{A}},l_{\bar{A}}} \delta_{k'_{\bar{A}},l'_{\bar{A}}} z_k \, z_{k'} \, \bar{z}_l \, \bar{z}_{l'}, \tag{4.6}$$

it is not difficult to express the potential as an average over bipartitions

$$H(\vec{\Phi}) = \binom{n}{n_A}^{-1} \sum_{|A|=n_A} H_A(\vec{\Phi}), \tag{4.7}$$

where

$$H_A(\vec{\Phi}) = \frac{N_c}{2} \sum_{k,k'} \sum_{\mu,\nu} \big(2\Phi^{\mu}_{k_A k_{\bar{A}}} \Phi^{\mu}_{k'_A k_{\bar{A}}} \Phi^{\nu}_{k'_A k'_{\bar{A}}} \Phi^{\nu}_{k_A k'_{\bar{A}}} - \Phi^{\mu}_{k_A k_{\bar{A}}} \Phi^{\nu}_{k'_A k_{\bar{A}}} \Phi^{\mu}_{k'_A k'_{\bar{A}}} \Phi^{\nu}_{k_A k'_{\bar{A}}}\big), \tag{4.8}$$

with $k_A = (k_i)_{i\in A}$.

Now, let

$$X_{k_{\bar{A}}\mu, l_{\bar{A}}\nu} = \sum_{k_A} \Phi^{\mu}_{k_A k_{\bar{A}}} \Phi^{\nu}_{k_A l_{\bar{A}}}, \tag{4.9}$$

and note that X is a symmetric $N_{\bar{A}} N_c \times N_{\bar{A}} N_c$ matrix, namely $X^T = X$. We get

$$H_A = \frac{N_c}{2} \sum_{k_{\bar{A}}, l_{\bar{A}}} \sum_{\mu,\nu} \big(2X^2_{k_{\bar{A}}\mu, l_{\bar{A}}\nu} - X_{k_{\bar{A}}\mu, l_{\bar{A}}\nu} X_{k_{\bar{A}}\nu, l_{\bar{A}}\mu}\big), \tag{4.10}$$

that is

$$H_A = \frac{N_c}{2} [2\,\mathrm{tr}(X^T X) - \mathrm{tr}(X^T Y)], \tag{4.11}$$

with $Y_{k_{\bar{A}}\mu, l_{\bar{A}}\nu} = X_{k_{\bar{A}}\nu, l_{\bar{A}}\mu}$ a symmetric matrix. By the Cauchy-Schwarz inequality for the Hilbert-Schmidt scalar product we get

$$\mathrm{tr}(X^T Y) \leqslant \mathrm{tr}(X^T X)^{1/2}\, \mathrm{tr}(Y^T Y)^{1/2}. \tag{4.12}$$

But it is easy to see that $\mathrm{tr}(Y^T Y) = \mathrm{tr}(X^T X)$, so that

$$H_A(\vec{\Phi}) \geqslant \frac{N_c}{2}\, \mathrm{tr}(X^2) > 0. \tag{4.13}$$

By making use of the constraint (4.5) we can estimate the positive lower bound as follows. First notice that the positive matrix $X \geqslant 0$ has unit trace. Indeed,

$$\mathrm{tr}\, X = \sum_{k_{\bar{A}},\mu} X_{k_{\bar{A}}\mu, k_{\bar{A}}\mu} = \sum_{k_A, k_{\bar{A}}, \mu} \Phi^{\mu}_{k_A, k_{\bar{A}}} \Phi^{\mu}_{k_A, k_{\bar{A}}} = 1, \tag{4.14}$$

by (4.5). Therefore,

$$\mathrm{tr}(X^2) \geqslant \frac{1}{\mathrm{rank} X} \geqslant \frac{1}{N_c N_{\bar{A}}}. \tag{4.15}$$

But, from the definition (4.9), we get that $\mathrm{rank}\, X \leqslant N_A$, so that

$$H_A(\vec{\Phi}) \geqslant \frac{N_c}{2N_A}. \tag{4.16}$$

By a straightforward computation, one can check that the minimum is attained at

$$\Phi^{\mu}_{k} = \frac{\phi^{\mu}}{\sqrt{N_A}} \delta_{k_{\bar{A}}, k_A}, \quad \sum_{\mu} (\phi^{\mu})^2 = 1, \tag{4.17}$$

where the Kronecker delta is meant to be 1 when $k_{\bar{A}} = (k_A, 0, \ldots, 0)$. Notice that (4.17) is the direct generalization of the maximally bipartite entangled state across the bipartition $(A, \bar{A})$, with coefficients $z_k = e^{i\alpha_k} \delta_{k_{\bar{A}}, k_A}/\sqrt{N_A}$.

By plugging (4.16) into (4.7) we finally get the desired lower bound

$$\min H \geqslant \frac{N_c}{2N_A}, \tag{4.18}$$

which may not be attained due to frustration among the bipartitions. See the discussion in Sec. V.

However, an interesting simplification occurs in the limit $N_c \to \infty$. We now introduce the constraint (4.5) by means of a Lagrange multiplier λ and rescale (for future purposes) the inverse fictitious temperature $\tilde{\beta} = \beta/\beta_0$, with

$$\beta_0 = \frac{2N^2}{N_A + N_{\bar{A}} - 1} \sim N^{3/2}. \tag{4.19}$$

We are finally left with the modified potential

$$\tilde{\beta}\mathcal{H}(\lambda) = \tilde{\beta}\beta_0 \frac{N_c}{2} \sum_{k,k',l,l'} \tilde{\Delta}(k,k';l,l')(\vec{\Phi}_k \cdot \vec{\Phi}_l)(\vec{\Phi}_{k'} \cdot \vec{\Phi}_{l'}) + \lambda \frac{N_c N}{2} \left(\sum_k \vec{\Phi}_k \cdot \vec{\Phi}_k - 1 \right). \tag{4.20}$$

The partition function is an integral over Φ and over the Lagrange multiplier imposing the constraint so that

$$Z = \int d\lambda\, d\Phi\, e^{-\tilde{\beta}\mathcal{H}(\lambda)}. \tag{4.21}$$

The evaluation of Z can be done by expanding it for small $\tilde{\beta}$ since the λ part is quadratic and, after resummation of the diagrams, calculating the saddle point in λ.

The saddle point equation in λ is

$$\frac{d}{d\lambda} \langle \mathcal{H} \rangle_{\beta} = 0 \tag{4.22}$$

and it is equivalent to the request that

$$\sum_k \langle \vec{\Phi}_k \cdot \vec{\Phi}_k \rangle_{\beta} = 1, \tag{4.23}$$

where the average is evaluated using the full partition function Z.

We should find the value of $\lambda(\tilde{\beta})$ that satisfies the constraint. For example, for $\tilde{\beta} = 0$ we have

$$G^{(0)\mu\nu}_{kl} = \left\langle \Phi^{\mu}_k \Phi^{\nu}_l \right\rangle_0 = \frac{1}{\lambda N_c N} \delta^{\mu\nu} \delta_{kl}, \tag{4.24}$$

where μ, ν are color indices; in order to satisfy the constraint we need $\lambda = 1$.

In the limit $N_c \to \infty$ the diagrams giving the dominant contribution are the cactuses. The solution for $\tilde{\beta} > 0$ can be obtained from the Dyson equation (Fig. 7) by considering only

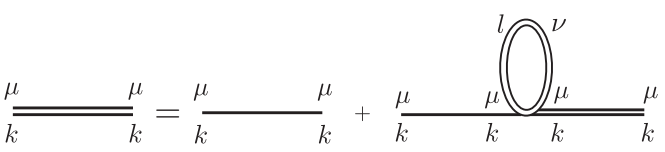

FIG. 7. Dyson equation for the propagator in the large-N_c limit.

the nonzero propagator, obtained by setting $\mu = \nu$, $k = l$, as

$$G^{\mu\mu}_{kk} = \left\langle \Phi^{\mu}_{k} \Phi^{\mu}_{k} \right\rangle_{\beta} = G^{(0)\mu\mu}_{kk} - \tilde{\beta}\beta_0 \frac{N_c}{2} G^{(0)\mu\mu}_{kk} \sum_{\nu,l} \tilde{\Delta}(k,l;k,l) G^{\nu\nu}_{ll} G^{\mu\mu}_{kk}. \tag{4.25}$$

From Eq. (4.24) we get

$$G^{\mu\mu}_{kk} = \frac{1}{\lambda N_c N} - \frac{\tilde{\beta}\beta_0}{2\lambda N} \sum_{\nu,l} \tilde{\Delta}(k,l;k,l) G^{\nu\nu}_{ll} G^{\mu\mu}_{kk}. \tag{4.26}$$

Let us define the quantity

$$G_l = \sum_{\nu=1}^{N_c} G^{\nu\nu}_{ll} \tag{4.27}$$

that, inserted into Eq. (4.26), gives

$$G^{\mu\mu}_{kk} = \frac{1}{N_c N} \frac{1}{\lambda + \frac{\tilde{\beta}\beta_0}{2N} \sum_l \tilde{\Delta}(k,l;k,l) G_l}. \tag{4.28}$$

We now sum over the color index μ and obtain

$$G_k = \frac{1}{N} \frac{1}{\lambda + \frac{\tilde{\beta}\beta_0}{2N} \sum_l \tilde{\Delta}(k,l;k,l) G_l}. \tag{4.29}$$

We also notice that the constraint (4.23) implies

$$\sum_{k \in \mathbb{Z}_2^n} G_k = 1. \tag{4.30}$$

For sufficiently small $\tilde{\beta}$, we look for a solution with unbroken permutation symmetry ($\mathcal{S}_N$ symmetric)

$$G_k = \frac{1}{N}, \quad \forall k \in \mathbb{Z}_2^n, \tag{4.31}$$

so that from Eq. (4.29) we have

$$\lambda + \frac{\tilde{\beta}\beta_0}{2N^2} \sum_l \tilde{\Delta}(k,l;k,l) = 1. \tag{4.32}$$

From Eqs. (2.6) and (4.3) we get

$$\sum_l \tilde{\Delta}(k,l;k,l) = \sum_l [2g(0,k \oplus l) - g(k \oplus l, k \oplus l)] = \sum_l [2g(0,l) - g(l,l)]. \tag{4.33}$$

For balanced bipartitions we obtain

$$\sum_l g(0,l) = \frac{N_A + N_{\bar{A}}}{2}, \quad \sum_l g(l,l) = 1, \tag{4.34}$$

so that

$$\sum_l \tilde{\Delta}(k,l;k,l) = N_A + N_{\bar{A}} - 1 \tag{4.35}$$

independent of k, and Eq. (4.32) reads

$$\lambda = 1 - \tilde{\beta}. \tag{4.36}$$

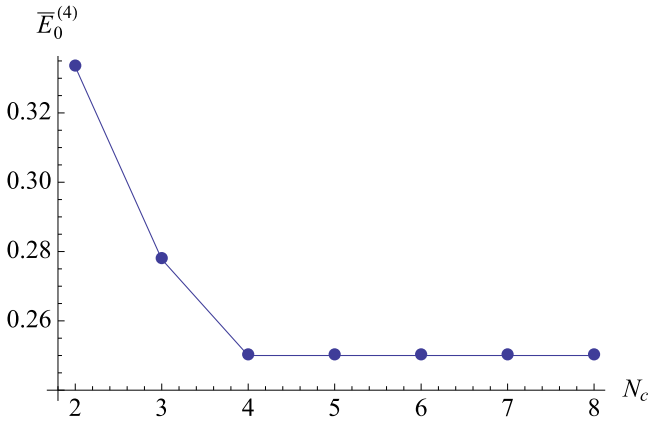

FIG. 8. (Color online) Dependence of the rescaled minimum $\bar{E}_0^{(n)}$ of the generalized potential (4.4) on the value of N_c for $n = 4$.

By using this result we get the average purity (again retaining only the leading order in $1/N_c$)

$$\langle H \rangle_{\beta} = \frac{N_c}{2} \sum_{k,l,\mu,\nu} \tilde{\Delta}(k,l,k,l) G^{\mu\mu}_{kk} G^{\nu\nu}_{ll} = \frac{N_c(N_A + N_{\bar{A}} - 1)}{2N} \sim \frac{N_c}{\sqrt{N}}, \tag{4.37}$$

independent of $\tilde{\beta}$ which, for $N_c = 2$, gives the correct result for the value of the first cumulant in Eq. (3.6) only at $\tilde{\beta} = 0$. This is due to the fact that, to the lowest order in $\tilde{\beta}$, subleading diagrams in N_c are subleading in N as well. Notice how, in this approximation, the dependence on the temperature has disappeared (a similar phenomenon occurs in a matrix model related to spin glasses [38]).

However, $\tilde{\beta} = 1$ is a critical temperature, as one can see that the Φ fluctuations become massless. In fact, the Lagrange multiplier λ is the coefficient of the quadratic part of the Hamiltonian (4.20),

$$\left. \frac{\partial^2 \mathcal{H}}{\partial \Phi^{\alpha}_k \partial \Phi^{\beta}_l} \right|_{\Phi=0} = \frac{1}{\tilde{\beta}} N_c N \delta^{\alpha\beta} \delta_{kl} \lambda. \tag{4.38}$$

Therefore, for $\tilde{\beta} > 1$, $\lambda < 0$ and for $N \to \infty$ we should expect spontaneous symmetry breaking such that, for some k, $\langle \Phi_k \rangle > 0$. The $\mathcal{S}_N$ symmetry gets spontaneously broken.

This value of $\tilde{\beta}_c$ is not in evident agreement with the numerics, although a tendency for large N_c of developing a kink at $\tilde{\beta} \sim 1$ is noted in the data for $n = 3$, 4, 5, and 7. In particular in Figs. 9, 10, 11, and 12 one notices that for small $\tilde{\beta}$ by increasing N_c the data move towards the large-N_c, small $\tilde{\beta}$, $\tilde{\beta}$-independent result (4.37), while for large $\tilde{\beta}$ the flow is reversed, probably asymptoting to the large-N_c minimum value of the generalized potential.

A complete solution of the partition function of the quartic Hamiltonian (4.20) and the $1/N_c$ corrections will be the subject of future work.

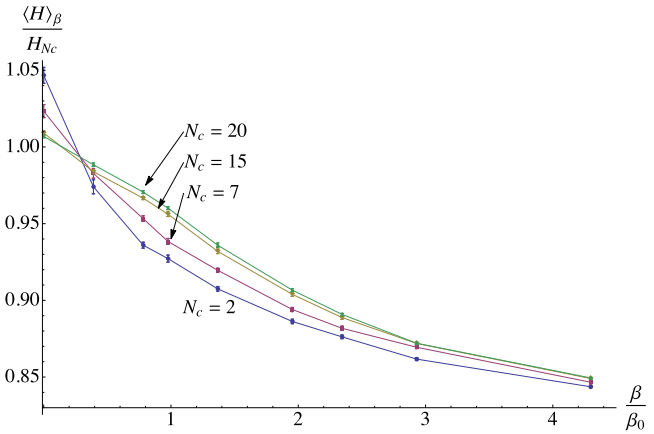

FIG. 9. (Color online) Numerical results for $n = 3$ ($N = 8$) and N_c ranging from 2 to 20. β_0 and H_{N_c} are defined in Eqs. (4.19) and (6.1).

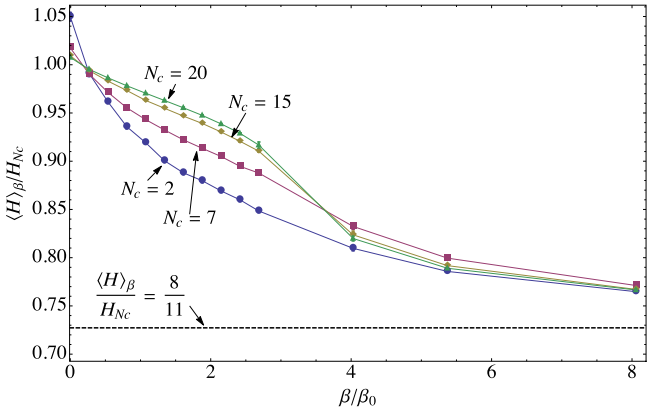

FIG. 11. (Color online) Numerical results for $n = 5$ ($N = 32$) and N_c ranging from 2 to 20. β_0 and H_{N_c} are defined in Eqs. (4.19) and (6.1).

V. MINIMUM OF THE POTENTIAL IN THE LARGE-N_c LIMIT

In this section we will give an explicit example of what happens to the potential of multipartite entanglement for increasing values of N_c.

Let us start by considering a collection of qubits. We recall that this case corresponds to $N_c = 2$. In particular, it is well known [11,23,24] that for $n = 4$ or $n \geqslant 8$, the ideal minimum of the potential of multipartite entanglement (4.4) cannot be reached, i.e.,

$$E_0^{(n)} = \min H \geqslant \frac{N_c}{2N_A} = \frac{N_c}{2} 2^{-[\frac{n}{2}]}, \tag{5.1}$$

where $[\cdot]$ denotes the integer part. We encounter the so-called *frustration of multipartite entanglement*. In other words the requirement that the bipartite entanglement is maximal (minimal purity) for all bipartitions can engender conflicts. Incidentally, we notice that this phenomenon can be found not only for spin systems but also for infinite-dimensional systems as in the case of Gaussian states [39].

In order to study this phenomenon, let us define the quantity

$$\bar{E}_0^{(n)} = \frac{2}{N_c} E_0^{(n)}, \tag{5.2}$$

which represents the rescaled minimum of the potential (4.4) for different values of N_c. In order to understand the consequence of the large-N_c limit, we have performed a numerical minimization of Eq. (4.4) for $n = 4$ and $2 \leqslant N_c \leqslant 8$. In Fig. 8 we plot $\bar{E}_0^{(n)}$ as a function of N_c. It is manifest that by increasing the value of the color parameter frustration disappears. Indeed, for $N_c = 2$ we find $\bar{E}_0^{(n)} = 1/3$, in agreement with previous results [15–17,19]. If $N_c \geqslant 4$ we have $\bar{E}_0^{(n)} = 1/4$. Apparently the ideal minimum is obtained by minimizing each term (4.8) in the generalized potential separately as if they were independent. Therefore, for $N_c \geqslant 4$ the system is *unfrustrated*. On the other hand, this means that one of the most characteristic trait of multipartite entanglement cannot be analyzed in the large-N_c limit.

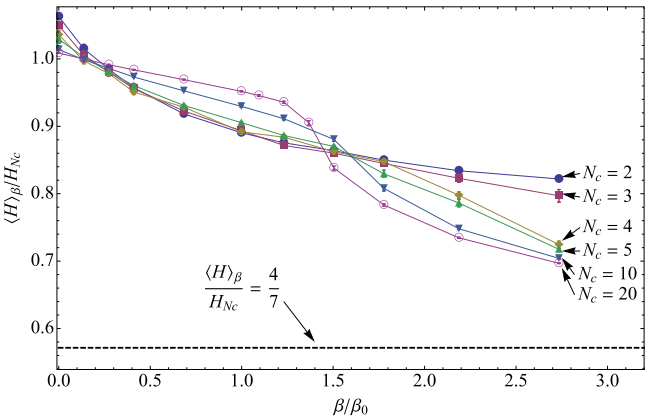

FIG. 10. (Color online) Numerical results for $n = 4$ ($N = 16$) and N_c ranging from 2 to 20. β_0 and H_{N_c} are defined in Eqs. (4.19) and (6.1).

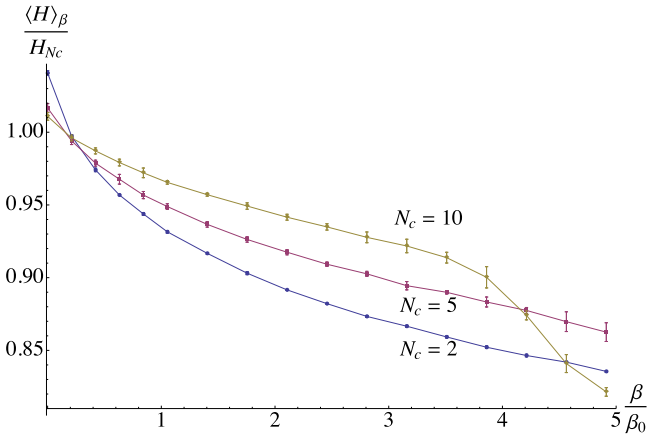

FIG. 12. (Color online) Numerical results for $n = 7$ ($N = 128$) and N_c ranging from 2 to 10. β_0 and H_{N_c} are defined in Eqs. (4.19) and (6.1).

Incidentally, it is interesting to notice that for $n = 4$ the values of the minimum potential follow the law

$$\bar{E}_0^{(4)} = \frac{N_c + 2}{6N_c} \tag{5.3}$$

and that for $N_c \geqslant 4$ this expression becomes $\leqslant 1/4$.

We emphasize that the case $n = 4$ qubits is far from being trivial and has been widely investigated in the literature. States that maximize the average purity for $n = 4$ do not necessarily maximize the von Neumann entropy [17]. It is also known that in the bipartite case, for large number of qubits, the order of the phase transition changes when one goes from the Renyi entropies to the von Neumann one [40]. Our analysis is restricted to the potential of multipartite entanglement (purity) and the von Neumann entropy is a limit that should be handled with care.

VI. SIGNATURES OF THE PHASE TRANSITION IN FINITE SYSTEMS

In the previous section we have found that a phase transition is observed in the large-N_c limit, when $\beta = \beta_0$ [see Eq. (4.36)]. In this section we will perform numerical calculations for finite systems (and finite N_c) and show where and how the signatures of this phase transition appear.

A. Search for the phase transition

In Figs. 9, 10, 11, and 12 [respectively for $n = 3$ ($N = 8$), $n = 4$ ($N = 16$), $n = 5$ ($N = 32$), and $n = 7$ ($N = 128$)] we plot the expectation value $\langle H \rangle_\beta$ rescaled by

$$H_{N_c} = \frac{N_c(N_A + N_{\bar{A}} - 1)}{2N} \tag{6.1}$$

versus $\tilde{\beta} = \beta/\beta_0$ for different values of the color number N_c obtained with Monte Carlo simulations. We recall that H is defined in Eq. (4.4) and β_0 in Eq. (4.19).

In all cases we notice that for large values of N_c there is an inflection point. Moreover, for increasing values of N_c, the curves tend to become flatter for small values of β/β_0. This behavior is more evident for $n = 4$ ($N = 16$) and $n = 7$ ($N = 128$). Finally, we notice that for $n = 4$ with $N_c > 3$ and $n = 7$ with $N_c = 10$ there is an evident change in the behavior of the curves for larger values of β/β_0, apparently absent in the case of $n = 5$. This could be due to the removal of the multipartite entanglement frustration in the case $n = 4$ as detailed in the previous section (the frustration phenomenon is not present for $n = 5$, and the case $n = 7$ is still open).

The flattening in the region of small $\tilde{\beta} = \beta/\beta_0$ is interpreted as a confirmation of the presence of a phase transition around $\tilde{\beta} = 1$ in the limit of large N_c. For $n = 4$ (where this effect is more evident) we notice that the inflection point of the curves moves from values of $\tilde{\beta} \simeq 2$ to $\tilde{\beta} \simeq 1.5$.

B. Hysteresis and replica overlaps

Having found clear signatures of the phase transition at finite N_c, N we now try to elucidate its features. In particular, we will search for the presence of hysteresis (in this context, associated with a first order phase transition) and we will study the overlap between parallel evolved replicas. To look

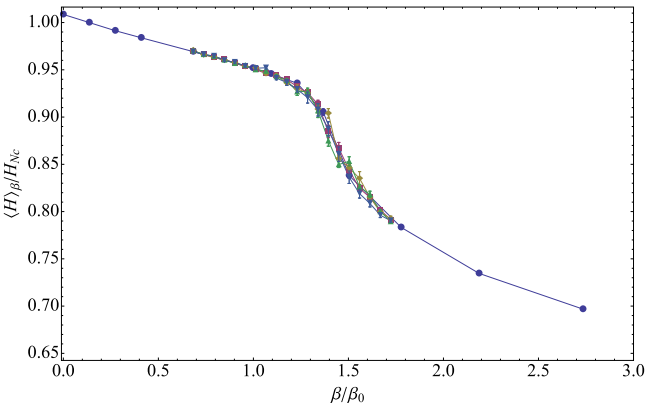

FIG. 13. (Color online) Search for the hysteresis phenomenon. Numerical results for $n = 4$ ($N = 16$), $N_c = 20$. β_0 and H_{N_c} are defined in Eqs. (4.19) and (6.1). Different curves correspond to different number of Monte Carlo steps between each decrease of β in the procedure. Blue dots: points for $N_c = 20$ shown in Fig. 10 (used as a reference); purple boxes: 300 Monte Carlo steps between different temperatures; yellow diamonds: 200 Monte Carlo steps between different temperatures; green triangles: 100 Monte Carlo steps between different temperatures; blue (upside down) triangles: 50 Monte Carlo steps between different temperatures. See the text for details.

for hysteresis we start from a large ("cool") initial value of β and we let the system reach equilibrium. At this point we start to "heat" the system and decrease the value of β fixing the number of Monte Carlo steps before the following decrease. We then cool back the system to the initial β. The analysis uses a simulated-annealing-like algorithm [41,42].

In Fig. 13 we show the results obtained for the case $n = 4$, $N_c = 20$. We start from $\beta = 130$ (point not shown in the figure), corresponding to $\beta/\beta_0 \simeq 1.8$, and anneal for 20 values of β (each step being equal to $\Delta\beta = 4$). The different curves correspond to 50, 100, 200, and 300 Monte Carlo steps before each decrease of β. Notice that the second procedure is what one calls quenching (as opposed to annealing). There is no evidence of hysteresis. As a reference, we have included in Fig. 13 also the curve (blue dots) that we have already included in Fig. 10: we remember that each point has been obtained not with simulated annealing but starting from $\beta = 0$, fixing the value of β, let the system reach the equilibration, and then performing a Monte Carlo run; the other curves in Fig. 13 are in excellent agreement with the case of $N_c = 20$ in Fig. 10. The annealing was repeated for 10 and 5 values of β instead of 20, and no substantial evidence of hysteresis appeared.

In order to compare the results using different procedures, we have tried to perform a simulated annealing procedure also going from $\beta = 0$ to larger values of the inverse temperature. We have changed the speed of the annealing procedure by varying the number of Monte Carlo steps between successive temperatures. The system is cooled starting from a given temperature, without going back to the initial state at every step. We expect to find the same results as in Fig. 13. We start from $\beta/\beta_0 = 0$ and then proceed with simulated annealing at steps $\simeq 0.1$ up to $\beta/\beta_0 = 3$ and then at steps $\simeq 1$ up to $\beta/\beta_0 = 10$. The rescaled potential for 500 Monte Carlo steps between different temperatures is plotted in Fig. 14, where

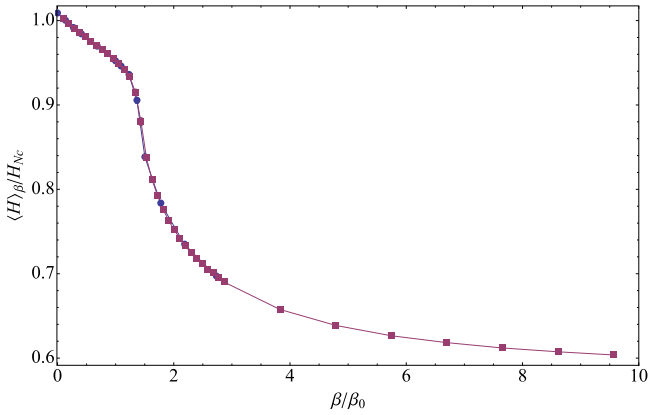

FIG. 14. (Color online) Numerical results for $n = 4$ ($N = 16$), $N_c = 20$, and 500 Monte Carlo steps (purple boxes). The data for the case $N_c = 20$ in Fig. 10 (blue dots) are used as a reference. β_0 and H_{N_c} are defined in Eqs. (4.19) and (6.1). See the text for details.

we show (blue dots) the curve obtained without the simulated annealing and the results using the simulated annealing (purple boxes). They corroborate our previous finding and extend the graph to larger values of β (below the frustrated minimum). No difference is observed for 100 Monte Carlo steps (not shown). We conclude that no hysteresis is present.

As a final test, we have considered the behavior of the *overlap* between configurations of two different Monte Carlo simulation run in parallel (labeled 1 and 2, respectively). This quantity is defined as

$$\langle q^2\rangle_\beta = \left\langle \left[\sum_k \vec{\Phi}_k^{(1)} \cdot \vec{\Phi}_k^{(2)} \right]^2 \right\rangle_\beta , \tag{6.2}$$

where the average is performed at a fixed value of β, by considering a configuration every ten Monte Carlo steps. We have considered the case of 500 Monte Carlo steps between different values of β. In order to check the robustness of the numerical results we performed ten different simulations and extracted only five overlaps. We observed a strong dependence on the choice of the pairing. In some cases we noticed a decrease of the overlap around $\beta/\beta_0 \simeq 2.5$, that most likely corresponds to different replicas freezing in different minima. In all cases, the overlaps remain bounded and never show any symptoms of possible divergencies. These results are indicative but not conclusive, due to the presence of large error bars and we will study this aspect of the problem in a future publication. It is also worth noticing that the error bars reduce significantly when $\beta/\beta_0 \leqslant 1.5$.

VII. CONCLUSIONS

We have investigated the behavior of the potential of multipartite entanglement by generalizing the problem to N_c colors and taking a large-N_c limit. In the analytical treatment we find that an instability occurs for sufficiently small temperatures that breaks the permutational symmetry between spin configurations. This instability generates, in the thermodynamic limit, a second order phase transition.

We have performed numerics for small system sizes ($n \leqslant 7, N_c \leqslant 20$) and observed the signatures of such phase transition (Sec. VI B). In order to exclude a first order transition, we have investigated the hysteresis phenomenon, not finding any signature of it. The quantitative comparison of the analytic, large-N_c results, with the numerics is plagued by large-N_c corrections (larger, the larger is n), but it is to a large extent satisfactory.

The frustration generated by the entanglement monogamy is to some extent similar to what happens in frustrated spin systems which have (for low temperatures) a glassy phase. However, it is worth remembering that our model does not contain any quenched disorder. Taking this into account, a more fit analogy is with configurational glasses [43–45].

Our result is of considerable significance for the physics of entanglement. Decreasing the temperature, the average of the potential of multipartite entanglement decreases towards its minimum. A smaller value of the potential is representative of a *more entangled state*. The typical states at low temperature are sampled from a measure which is not $\mathcal{S}_n$ symmetric, so the states which minimize the potential are necessarily concentrated on fewer spin configurations. This is at first thought counterintuitive. One might think that in order to get *more* multipartite entanglement one should mix in more configurations and create a more uniform wave vector on the binary hypercube $\mathbb{Z}_2^n$. We show that the opposite is true. The states which maximize the multipartite entanglement have a certain degree of breaking of the $\mathcal{S}_n$ symmetry.

Finally, there are other features of entanglement frustration that have not been analyzed in this article, that pertain to the ground states of some quantum many-body Hamiltonians [46–51]. As entanglement is a resource for quantum computation, it would be desirable to see if one can find a quantum Hamiltonian whose ground state is highly entangled. In this direction, recent developments have shown that some quantum many-body Hamiltonians [52–54] made from projectors [55,56] do violate the common area law for entanglement in favor of volume or almost-volume law. These ground states are likely candidates for quantum certificates of difficult quantum computation problems.

ACKNOWLEDGMENTS

This work was partially supported by PRIN 2010LLKJBX on "Collective quantum phenomena: from strongly correlated systems to quantum simulators," and by the Italian National Group of Mathematical Physics (GNFM-INdAM, Progetto Giovani). We acknowledge the Bc^2S-RECAS farm (Università di Bari and INFN) for computational resources. A.S. would like to thank "Università di Bari" for hospitality and financial support during the completion of this work.

[1] A. Einstein, B. Podolsky, and N. Rosen, Phys. Rev. **47**, 777 (1935).

[2] E. Schrödinger, Proc. Cambridge Philos. Soc. **31**, 555 (1935); **32**, 446 (1936).

[3] W. K. Wootters, Quantum Inf. Comput. **1**, 27 (2001).
[4] L. Amico, R. Fazio, A. Osterloh, and V. Vedral, Rev. Mod. Phys. **80**, 517 (2008).
[5] R. Horodecki, P. Horodecki, M. Horodecki, and K. Horodecki, Rev. Mod. Phys. **81**, 865 (2009).
[6] M. A. Nielsen and I. L. Chuang, *Quantum Computation and Quantum Information* (Cambridge University Press, Cambridge, 2000).
[7] I. Bengtsson and K. Życzkowski, *Geometry of Quantum States* (Cambridge University Press, Cambridge, 2006).
[8] D. A. Meyer and N. R. Wallach, J. Math. Phys. **43**, 4273 (2002).
[9] V. I. Manko, G. Marmo, E. C. G. Sudarshan, and F. Zaccaria, J. Phys. A **35**, 7137 (2002).
[10] M. Mezard, G. Parisi, and M. A. Virasoro, *Spin Glass Theory and Beyond* (World Scientific, Singapore, 1987).
[11] P. Facchi, G. Florio, U. Marzolino, G. Parisi, and S. Pascazio, New J. Phys. **12**, 025015 (2010).
[12] V. Coffman, J. Kundu, and W. K. Wootters, Phys. Rev. A **61**, 052306 (2000).
[13] T. J. Osborne and F. Verstraete, Phys. Rev. Lett. **96**, 220503 (2006).
[14] B. Regula, S. Di Martino, S. Lee, and G. Adesso, Phys. Rev. Lett. **113**, 110501 (2014).
[15] G. Gour and N. R. Wallach, J. Math. Phys. **51**, 112201 (2010).
[16] A. Higuchi and A. Sudbery, Phys. Lett. A **273**, 213 (2000).
[17] A. Borras, M. Casas, A. R. Plastino, and A. Plastino, Int. J. Quantum Inf. **06**, 605 (2008).
[18] V. M. Kendon, K. Nemoto, and W. J. Munro, J. Mod. Opt. **49**, 1709 (2002).
[19] I. D. K. Brown, S. Stepney, A. Sudbery, and S. L. Braunstein, J. Phys. A **38**, 1119 (2005).
[20] A. Osterloh and J. Siewert, Int. J. Quantum. Inform. **04**, 531 (2006).
[21] A. Borras, A. R. Plastino, J. Batle, C. Zander, M. Casas, and A. Plastino, J. Phys. A **40**, 13407 (2007).
[22] S. Brierley and A. Higuchi, J. Phys. A **40**, 8455 (2007).
[23] A. J. Scott, Phys. Rev. A **69**, 052330 (2004).
[24] P. Facchi, G. Florio, G. Parisi, and S. Pascazio, Phys. Rev. A **77**, 060304(R) (2008).
[25] P. Facchi, Rend. Lincei Mat. Appl. **20**, 25 (2009).
[26] L. Arnaud and N. J. Cerf, Phys. Rev. A **87**, 012319 (2013).
[27] D. Goyeneche and K. Życzkowski, Phys. Rev. A **90**, 022316 (2014).
[28] P. Facchi, G. Florio, and S. Pascazio, Phys. Rev. A **74**, 042331 (2006).
[29] P. Facchi, G. Florio, U. Marzolino, G. Parisi, and S. Pascazio, J. Phys. A: Math. Theor. **42**, 055304 (2009).
[30] P. Facchi, G. Florio, U. Marzolino, G. Parisi, and S. Pascazio, J. Phys. A **43**, 225303 (2010).
[31] A. De Pasquale, P. Facchi, V. Giovannetti, G. Parisi, S. Pascazio, and A. Scardicchio, J. Phys. A **45**, 015308 (2012).
[32] P. Facchi, U. Marzolino, G. Parisi, S. Pascazio, and A. Scardicchio, Phys. Rev. Lett. **101**, 050502 (2008).
[33] A. De Pasquale, P. Facchi, G. Parisi, S. Pascazio, and A. Scardicchio, Phys. Rev. A **81**, 052324 (2010).
[34] K. Życzkowski and H.-J. Sommers, J. Phys. A **34**, 7111 (2001).
[35] G. 't Hooft, Nucl. Phys. B **75**, 461 (1974).
[36] E. Brézin, C. Itzykson, G. Parisi, and J. B. Zuber, Commun. Math. Phys. **59**, 35 (1978).
[37] M. Moshe and J. Zinn-Justin, Phys. Rep. **385**, 69 (2003).
[38] L. F. Cugliandolo, J. Kurchan, G. Parisi, and F. Ritort, Phys. Rev. Lett. **74**, 1012 (1995).
[39] P. Facchi, G. Florio, C. Lupo, S. Mancini, and S. Pascazio, Phys. Rev. A **80**, 062311 (2009).
[40] P. Facchi, G. Florio, G. Parisi, S. Pascazio, and K. Yuasa, Phys. Rev. A **87**, 052324 (2013).
[41] S. Kirkpatrick, C. D. Gelatt, and M. P. Vecchi, Science **220**, 671 (1983).
[42] D. P. Landau and K. Binder, *A Guide to Monte Carlo Simulations in Statistical Physics* (Cambridge University Press, Cambridge, 2009).
[43] E. Marinari, G. Parisi, and F. Ritort, J. Phys. A **27**, 7615 (1994).
[44] E. Marinari, G. Parisi, and F. Ritort, J. Phys. A **27**, 7647 (1994).
[45] I. Borsari, M. Degli Esposti, S. Graffi, and F. Unguendoli, J. Phys. A **30**, 155 (1997).
[46] C. M. Dawson and M. A. Nielsen, Phys. Rev. A **69**, 052316 (2004).
[47] M. M. Wolf, F. Verstraete, and J. I. Cirac, Int. J. Quantum. Inform. **01**, 465 (2003).
[48] N. de Beaudrap, M. Ohliger, T. J. Osborne, and J. Eisert, Phys. Rev. Lett. **105**, 060504 (2010).
[49] J. Schnack, Dalton Trans. **39**, 4677 (2010).
[50] S. M. Giampaolo, G. Adesso, and F. Illuminati, Phys. Rev. Lett. **104**, 207202 (2010).
[51] U. Marzolino, S. M. Giampaolo, and F. Illuminati, Phys. Rev. A **88**, 020301(R) (2013).
[52] S. Bravyi, L. Caha, R. Movassagh, D. Nagaj, and P. W. Shor, Phys. Rev. Lett. **109**, 207202 (2012).
[53] R. Movassagh, E. Farhi, J. Goldstone, D. Nagaj, T. J. Osborne, and P. W. Shor, Phys. Rev. A **82**, 012318 (2010).
[54] R. Movassagh and P. W. Shor, arXiv:1408.1657.
[55] C. R. Laumann, R. Moessner, A. Scardicchio, and S. L. Sondhi, in *Modern Theories of Many-Particle Systems in Condensed Matter Physics* (Springer, Berlin, 2012), pp. 295–332.
[56] C. R. Laumann, R. Moessner, A. Scardicchio, and S. L. Sondhi, Quantum Inf. Comput. **10**, 1 (2010).